Chapter 1
Chimera states in pulse coupled neural networks:
the influence of dilution and noise

Simona Olmi and Alessandro Torcini

We analyse the possible dynamical states emerging for two symmetrically pulse coupled populations of leaky integrate-and-fire neurons. In particular, we observe broken symmetry states in this set-up: namely, breathing chimeras, where one population is fully synchronized and the other is in a state of partial synchronization (PS) as well as generalized chimera states, where both populations are in PS, but with different levels of synchronization. Symmetric macroscopic states are also present, ranging from quasi-periodic motions, to collective chaos, from splay states to population anti-phase partial synchronization. We then investigate the influence disorder, random link removal or noise, on the dynamics of collective solutions in this model. As a result, we observe that broken symmetry chimera-like states, with both populations partially synchronized, persist up to 80% of broken links and up to noise amplitudes $\simeq 8\%$ of threshold-reset distance. Furthermore, the introduction of disorder on symmetric chaotic state has

Simona Olmi

Aix Marseille Univ, Inserm, INS, Institut de Neurosciences des Systémes, Marseille, France;
CNR - Consiglio Nazionale delle Ricerche - Istituto dei Sistemi Complessi, 50019 Sesto Fiorentino, Italy;
INFN - Istituto Nazionale di Fisica Nucleare - Sezione di Firenze, 50019 Sesto Fiorentino, Italy.
e-mail: simona.olmi@univ-amu.fr

Alessandro Torcini

Aix Marseille Univ, Inserm, INMED, Institute de Neurobiologie de la Méditerranée and INS, Institut de Neurosciences des Systémes, Marseille, France;
Aix-Marseille Université, Université de Toulon, CNRS, CPT, UMR 7332, 13288 Marseille, France;
CNR - Consiglio Nazionale delle Ricerche - Istituto dei Sistemi Complessi, 50019 Sesto Fiorentino, Italy.
e-mail: alessandro.torcini@univ-amu.fr

```
a constructive effect, namely to induce the emergence of
chimera-like states at intermediate dilution or noise level.
```

1.1 Introduction

The emergence of broken symmetry states (*Chimera states*) in population of os-
cillators or rotators is an extremely popular and active research field nowdays, in
particular after that experimental evidences for the existence of these states have
been reported in several contexts ranging from ensembles of mechanical oscillators,
to laser dynamics, to populations of chemical oscillators (for a recent review on the
subject see [14]). Chimera states in neural systems have been firstly reported by Sak-
aguchi for a chain of nonlocally coupled Hodgkin-Huxley models with excitatory
and inhibitory synaptic coupling [18], while the first evidence of chimeras in models
of globally coupled populations has been reported in [12] for leaky integrate-and-
fire (LIF) excitatory neurons. More recently, chimeras in LIF networks have anal-
ysed in different contexts, ranging from small-network topology [17], to chains of
non-locally coupled LIFs with refractoriness [20], to the emergence of chimeras in a
single fully coupled neural population [4]. Globally pulse coupled Winfree models,
reproducing θ-neuron dynamics, also support chimera states, ranging from breath-
ing (periodic and quasi-periodic) to chaotic ones [15].

Since the connectivity in the brain is definitely sparse and noise sources cannot be
avoided, it is fundamental in order to understand the possible relevance of chimera-
like states in neural dynamics to test for the robustness of these solutions to dilution
and to the presence of noise. Studies in this direction have been performed mainly
for oscillator models [6, 7, 8] or excitable systems [19]. In particular, chimera states
in random diluted Erdös-Renyi networks have been observed up to a dilution of 8%
of the links [6], furthermore it has been shown that noise has not only a washing out
effects on chimera solutions, but it can also have a constructive role promoting new
dynamical phenomena [7, 19].

In this paper, we focus on the dynamics of two fully pulse coupled populations
of excitatory LIF neurons with stronger synaptic coupling among the neurons of the
same population and a weaker coupling with those of the other population, similarly
to the simplest set-up showing the emergence of chimera states in phase oscillator
networks [1]. Furthermore, the neurons are synaptically connected via the transmis-
sion of pulses of finite duration. This model for globally coupled systems reveal the
emergence of broken symmetry population states, chimera-like, [12], as well as of
chimera states even within a single population [4].

Our main aim is to study how the macroscopic solutions, found in the determin-
istic fully coupled networks, will be modified by considering randomly connected
networks of increasing dilution and by adding noise of increasing amplitude to the
system. In particular, after having introduced the considered models in Sect. 1.2, we
will report the complete phase diagram for the macroscopic solutions of the fully
coupled case in Sect. 1.3. These solutions vary from chimera-like, to symmetric so-

lutions with complex dynamic ranging from collective quasi-periodic dynamics to macroscopic chaos. Furthermore, we will concentrate on the effect of random dilution and noise on the dynamics of broken symmetry and chaotic states in Sect. 1.4 and 1.5. Finally, we will devote Sect. 1.6 to a brief discussion of the reported results. The algorithm employed to exactly integrate the fully coupled populations is explained in the Appendix.

1.2 The model

Firstly we consider two fully coupled networks, each made of N LIF oscillators. Following Refs. [23], the membrane potential $x_j^{(k)}(t)$ of the $j-th$ oscillator ($j = 1, \ldots, N$) of the kth population ($k = 0, 1$) evolves according to the differential equation,

$$\dot{x}_j^{(k)}(t) = a - x_j^{(k)}(t) + g_s E^{(k)}(t) + g_c E^{(1-k)}(t) \tag{1.1}$$

where $a > 1$ is the suprathreshold input current, while $g_s > 0$ and $g_c > 0$ gauge the self- and, resp., cross-coupling strength of the excitatory interaction. The discharge mechanism operating in real neurons is modeled by assuming that when the membrane potential reaches the threshold value $x_j^{(k)} = x_{th} = 1$, it is reset to the value $x_j^{(k)} = x_R = 0$, while a α-pulse $p(t) = \alpha^2 t \exp -\alpha t$ is transmitted to and instantaneously received by the connected neurons. For this kind of pulses the field $E^{(k)}(t)$ generated by the neurons of the population k, satisfies the differential equation

$$\ddot{E}^{(k)}(t) + 2\alpha\dot{E}^{(k)}(t) + \alpha^2 E^{(k)}(t) = \frac{\alpha^2}{N} \sum_{j,n} \delta(t - t_{j,n}^{(k)}) , \tag{1.2}$$

where $t_{j,n}^{(k)}$ is the nth spiking time of the jth neuron within the population k, and the sum is restricted to times smaller than t. In the limit case $g_s = g_c = g$, the two populations can be seen as a single one made of $2N$ neurons with an effective coupling constant $G = 2g$.

Secondly we consider two random undirected Erdös-Renyi networks, each made of N LIF oscillators and with an average in-degree K, therefore the probability to have a link between two neuron is simply K/N. We assume that the membrane potential $x_j^{(k)}(t)$ of the $j-th$ oscillator of the kth population ($k = 0, 1$) evolves according to the differential equation

$$\dot{x}_j^{(k)}(t) = a - x_j^{(k)}(t) + g_s E_j^{(k)}(t) + g_c \overline{E}^{(1-k)}(t) \quad ; \tag{1.3}$$

where the field $E_j^{(k)}(t)$ takes in account of the pulses received by neuron j from neurons of its own population, while the field $\overline{E}^{(1-k)}(t)$ represents the effect of the neuron beloging to the other population.

In particular, $E_j^{(k)}(t)$ is the linear superposition of the pulses $p(t)$ received by neuron i of the kth-population at all times $t_n < t$ (the integer index n orders the sequence of the pulses emitted in the network), namely :

$$E_j^{(k)}(t) = \frac{1}{K}\sum_i \sum_{n|t_n<t} C_{i(n),j}^{(k)}\theta(t-t_n)p(t-t_n) \quad , \tag{1.4}$$

where $\theta(x)$ is the Heavyside function and the connectivity matrix $C_{i,j}^{(k)}$ has entries 1 (0) depending if the neuron j presents a post-synaptic neuron connection with neuron i or not. For each neuron we should introduce a different field, since each neuron has a different connectivity in the network. It is more convenient to turn also this time, as previously done for the globally coupled case, the explicit Eq. (1.4) into the following differential equation

$$\ddot{E}_j^{(k)}(t) + 2\alpha\dot{E}_j^{(k)}(t) + \alpha^2 E_j^{(k)}(t) = \frac{\alpha^2}{K}\sum_{i,n} C_{i(n),j}^{(k)}\delta(t-t_{i,n}^{(k)}) \, . \tag{1.5}$$

Furthermore, $\overline{E}^{(1-k)}(t) = \frac{1}{N}\sum_{i=1}^N E_i^{(1-k)}(t)$ represents a "mean field" effect of the second population on the neuron of the first population, since it is the average of all the fields $E_i^{(1-k)}$ of the second population. As a result, the dynamics of the neural network model takes the more "canonical" form of a set of coupled ordinary differential Eqs. (1.3) and (1.5), which can be analyzed with the standard methods of dynamical systems. The setup we have employed, diluted random connectivity within each population, but mean-field like cross coupling, will favour the stabilization of the broken symmetry state as suggested in [6]. The have studied the diluted networks in so-called massively connected case, namely where the average in-degree is proportional to the system size $K = (1-d) \times N$.

Finally we consider two diluted networks with noise. The noise is introduced in the system every time the membrane potential has reached the threshold value and it is reset to the reset value. In particular, instead of using a reset value $x_R = 0$, the neuron is reset to a random value chosen in the interval $x_R \in [-\Delta, \Delta]$, where Δ takes into account the level of the noise. In this case the percentage of dilution is kept fixed ($d = 0.2$).

The integration of the above models is performed exactly in terms of so-called event driven maps analogously to what previously done in [23, 12], for the two fully coupled cases, where non trivial round-off problems can occur a more refined event driven map has been developed and it is explained in the Appendix.

The degree of synchronization within each population of neurons can be quantified by introducing the typical order parameter used for phase oscillators $r^{(k)}(t) = |\langle e^{i\theta_j^{(k)}(t)}\rangle|$, where $\theta_j^{(k)}$ is the phase of the jth oscillator, that can be properly defined as a (suitably scaled) time variable [22], $\theta_j^{(k)}(t) = 2\pi(t-t_{j,n}^{(k)})/(t-t_{m,n-1}^{(k)})$, where n identifies the time of the last spike emitted by the jth neuron, while m identifies the neuron that has emitted the last spike at time t. One can verify that this phase is

bounded between 0 and 2π, as it should. Furthermore, the fully synchronized regime corresponds to $r^{(k)} \equiv 1$, and in the asynchronous regime one expects $r^{(k)} \simeq 1/\sqrt{K}$, where K is the average in-degree of the network.

1.3 Fully Coupled Network: Phase Diagram
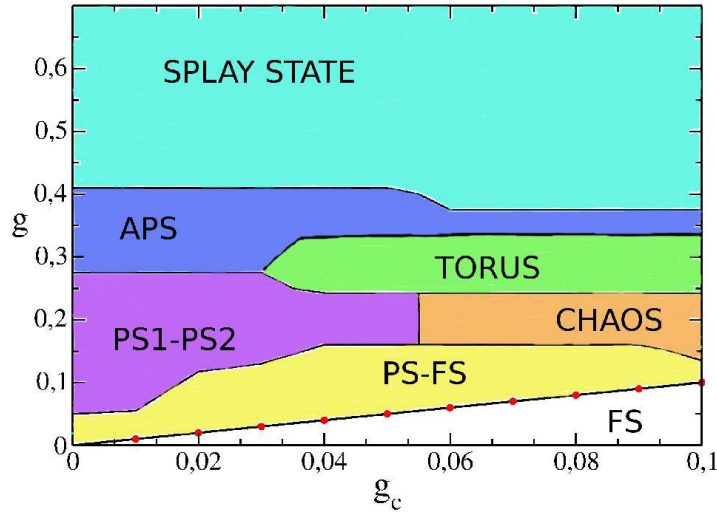
Fig. 1.1 (Color Online) Phase diagram in the (g_c, g_s)-plane reporting the stability region of the observed various collective solutions. For the definitions of the different phases see the text.

The phase plane (g_c, g_s) shown in Fig. 1.1 has been obtained by studying the model (1.1,1.2) for $a = 1.3$ and $\alpha = 9$. As already mentioned, along the diagonal $(g = g_s = g_c)$ the two population model (1.1) reduces to a single population with coupling strength $G = 2g$. For our choice of a and α values, the system exhibits *Partial Sybnchronization* PS, where the macroscopic field displays collective periodic oscillations and the microscopic dynamics is quasiperiodic [21, 23]. Below the diagonal, the evolution is still symmetric but the neurons are now *Fully Synchronized* (FS); the neurons of both populations fire at the unison. More interesting phenomena can be observed above the diagonal. In this situation a solution with broken symmetry emerges naturally, where one population is FS and the other is PS, this represents a generalized form of chimera state. In particular, one observes that while the order parameter of one population is exactly one, the other oscillates periodically, as shown in Fig. 1.2 (c). Therefore this chimera state can be classified as a *periodically breathing chimera*, which has been previously reported for the Kuramoto model [1, 16] as well as for a two population network of rotators in [13]. De-
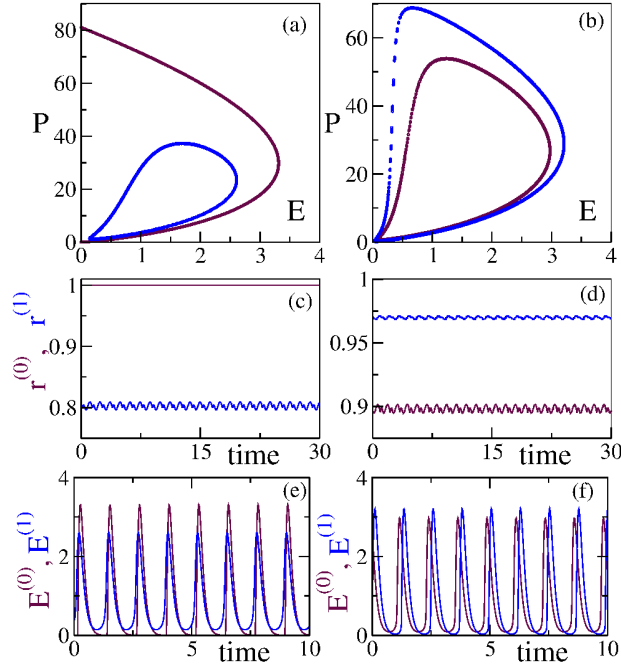
Fig. 1.2 (Color Online) Macroscopic attractors displayed by reporting $P \equiv E + \alpha \dot{E}$ vs E for a PS-FS state (a) and a PS1-PS2 (b), the time evolution of the corresponding order parameters $r^{(0)}$ and $r^{(1)}$ is also reported in (c) and (d). In panels (e), (f) are reported the time behaviors of the macroscopic fields $E^{(0)}$ and $E^{(1)}$. The variables corresponding to population 0 (resp. 1) are shown in blue (resp. maroon). As regards the parameter values, $(g_c = 0.07, g_s = 0.1)$ in (a),(c) and $(g_c = 0.02, g_s = 0.17)$ in (b),(d).

spite the macroscopic filds $E^{(0)}$ and E^1 are both oscillating periodically and locked, as evident from Figs. 1.2 (a),(e), the two populations are characterized by different behaviour at a microscopic level, where the neurons are periodic in the FS population and quasi-periodic in the PS population. This means that the neurons subject to two different linear combinations of $E^{(0)}$ and $E^{(1)}$ behave differently: a population locks with the forcing field, while the other one behaves quasi-periodically.

Another even more interesting symmetry broken state (termed PS1-PS2) can be observed for larger g_s-values and $g_c < 0.055$; in this case both populations exhibit PS, but their dynamics take place over two different attractors with two different degrees of synchronization, as shown in Fig. 1.2 (b),(d). Analogously to the PS-FS state, the two fields are periodic and phase locked, as it can be seen by looking at the time behavior of $E^{(0)}$ and $E^{(1)}$ in Fig. 1.2 (f). However, at variance with PS-FS, here both populations exhibit quasi-periodic motions. This simmetry broken state can be also considered a Chimera state and it has been reported only for LIF populations so-far [12].
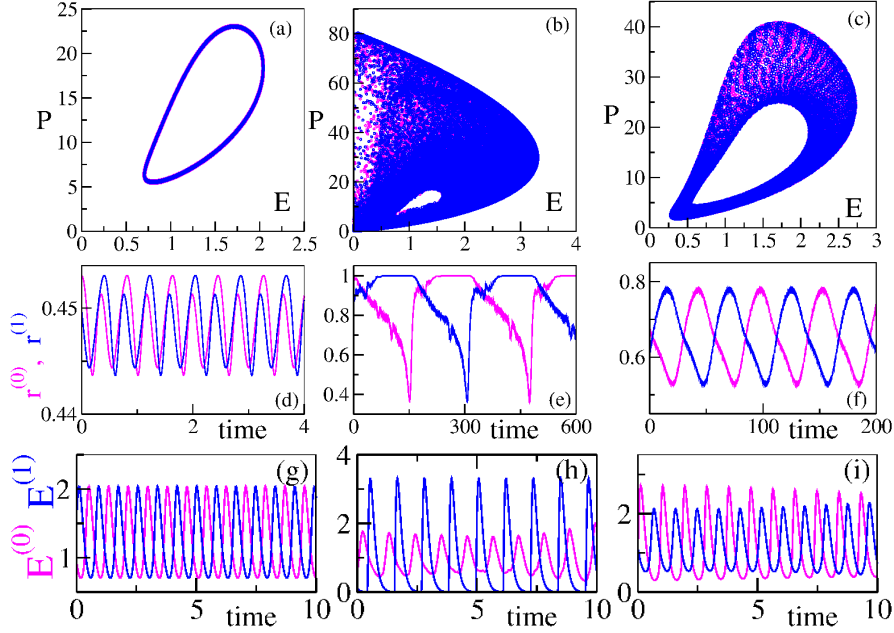
Fig. 1.3 (Color Online) Macroscopic attractors displayed by reporting $P \equiv E + \alpha\dot{E}$ vs E for an APS (a), a chaotic state (b), and a TORUS state (c), the time evolution of the corresponding order parameters $r^{(0)}$ and $r^{(1)}$ is also reported in (d), (e) and (f). In panels (g), (h), (i) are reported the time behaviors of the macroscopic fields $E^{(0)}$ and $E^{(1)}$. The variables corresponding to population 0 (resp. 1) are shown in magenta (resp. blue). As regards the parameter values, $(g_c = 0.07, g_s = 0.35)$ in (a),(d),(g), $(g_c = 0.08, g_s = 0.16)$ in (b),(e),(h) and $(g_c = 0.07, g_s = 0.3)$ in (c),(f),(i).

For larger g_s values the symmetry between the two collective fields is recovered with the only difference of phase shift between the two fields which oscillate in antiphase and this is why we term this regime *Antiphase Partial Synchronization* (APS) (see Fig. 1.3 (a), (g)). In this regime, at finite N the istantaneous maximum Lyapunov exponent strongly fluctuates and we cannot exclude that this regime is *weakly chaotic*. Analogously to the chaotic behaviour found in single population of massively coupled LIFs [11], we expect that the chaoticity disappears in the thermodynamic limit. However, it is peculiar the behaviour of the order parameters in this case, as shown in Fig. 1.3 (d): the two populations are not equally synchronized and the two order parameters $r^{(0)}$ and $r^{(1)}$ are behaving periodically in time, but at each oscillation the role of most synchronized population switches from one to the other.

In a limited region above the diagonal and for $g_c > 0.055$ the collective behaviour is still symmetric but irregular (*Collective Chaos*), as revelead by the two macroscopic attractors (see Fig. 1.3(b)). Furthermore, in this case one can observe quite wide oscillations of the order parameters of the two populations in the range $0.4 \leq r^{(0)}, r^{(1)} \leq 1$, as shown in Fig. 1.3(c). Whenever one population gets synchronized, with an order parameter $\simeq 1$, the other partially desynchronizes reaching val-

ues $r \simeq 0.4$. These collective oscillations in the order parameters occur on quite long timescale with respect to the periods of oscillations of the two macroscopic field $E^{(0)}$ and $E^{(1)}$ reported in Fig. 1.3(h). However, the oscillations in the level of synchronization induce modulations with periods of the same order in the field dynamics. In a previous paper [12] we have demonstrated that the finite-amplitude Lyapunov exponent [3], for this state, coincides with the microscopic maximal Lyapunov exponent, thus suggesting that the microscopic chaos is induced by the collective drive and therefore the origin of chaos is indeed collective in this case.

Moreover, in a strip above the chaotic region, one can observe a symmetric collective quasiperiodic motion on a *Torus* T^2 for both populations (see Fig. 1.3 (c)). This means that the quasiperiodic motion of the fields is accompanied by a dynamics of the single neurons along a torus T^3. An analogous regime has been previously reported in [10] for a population of coupled Stuart-Landau oscillators. Here, we find it in a model where the single units are described by an single variable. Furthermore, the motion on the macroscopic T^2 attractor reported in Fig. 1.3 (c) can be characterized by estimating the winding numbers for various system sizes, we observe that the winding number is constant, indicating that the torus survives in the thermodynamic limit. In this case, we observe quite regular antiphase oscillations in the synchronization order parameters between values $0.4 \leq r^{(0)}, r^{(1)} \leq 0.8$ occurring on time scales definitely longer than those associated to the oscillations of the macroscopic fields (as shown in Fig. 1.3 (f) and (i).

Finally, for yet larger g_s-values both populations converge towards a *Splay State*, characterized by constant fields, no collective motion and periodic microsocpic evolution of the neurons. This is not surprising, as we already know that for the chosen α- and a-values, the splay state is stable in a single population of neurons for $G > G_0 \equiv 0.425$ [21, 23].

1.4 Diluted Networks

In order to observe the influence of dilution on the dynamics, we considered in absence of dilution a PS-FS state with broken symmetry and a Chaotic state. In particular, we have analyzed the modifications of the macroscopic attractors, of the level of synchronization, as well as the microscopic dynamics induced by cutting randomly links for these 2 states.

To characterize the two macroscopic states, we have decided to consider the level of synchronization in the two populations. In general, we observe that the effect of dilution is, as expected, to reduce the level of synchronization in the system. In particular, starting from the PS-FS state in the fully coupled case, the average values $\bar{r}^{(0)}$ and $\bar{r}^{(1)}$ remain distinct up to some critical dilution $d_c \simeq 0.75$ (as shown in Fig. 1.5 (a)). For intermediate values of the dilution, in the range $0.2 \leq d \leq d_c$, a broken symmetry state is still observable, characterized by two periodically oscillating fields with associated different attractors (see Figs 1.4 (a),(e), and (o)). Therefore, we can safely classify this as a chimera PS1-PS2 state, despite the dilution induces
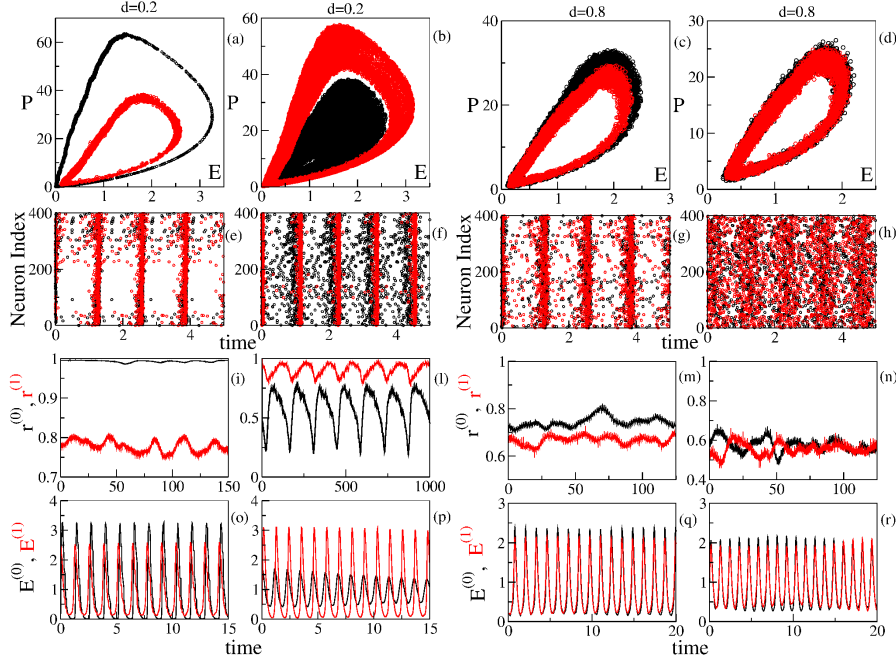
Fig. 1.4 (Color Online) **Influence of Dilution.** Macroscopic and microscopic characterization for two different dilutions (namely $d = 0.2$ and 0.8) of two states that at $d = 0$ were FS-PS (first and third columns) and chaotic (second and fourth columns). In the first row the corresponding macroscopic attractors are reported, namely, $P \equiv E + \alpha \dot{E}$ vs E are shown; the raster plots are shown in the second row; the time evolution of the order parameters $r^{(0)}$ and $r^{(1)}$ is reported in the third row, while that of the macroscopic fields $E^{(0)}$ and $E^{(1)}$ is shown in the forth row. The variables corresponding to population 0 (resp. 1) are shown in black (resp. red). As regards the parameter values, $(g_c = 0.04, g_s = 0.1)$ for the first and third columns, and $(g_c = 0.08, g_s = 0.16)$ for the second and fourth columns. The employed values of dilution are reported over the corresponding columns.

fluctuations in the macroscopic fields [11, 2]. For larger dilution, above the critical value, the two attractors essentially merge (as shown in Figs 1.4 (i)), but both the macroscopic fields are still presenting clear collective periodic oscillations even at these levels of dilution (see Figs 1.4 (c)), confirming the robustness of the PS states in this model.

As a general remark when we considered the influence of dilution on a PS1-PS2 state , we observed a similar scenario, obviously without an initial window where the FS was still observable.

The dilution has a quite peculiar effect on the chaotic, symmetric, state; in fact, up to dilution $d \simeq 0.2$, we did not observe any new effect, as evidenced by the average value of the synchronization order parameters reported in Fig. 1.5 (b). However, already at $d = 0.2$ the dilution induce a symmetry break among the two population dynamics. This is clear in Fig. 1.4 (b), where one population is still in a collective chaotic state, similar to the one observed for the globally coupled system, while

the other reveals an attractor analogous to the one seen for the PS state. This is even more evident by considering the time evolution of the order parameters, while one population exhibits large oscillations of $r^{(0)}$, similar to the one observed for the chaotic state, the other reveals more limited oscillations (see Fig. 1.4 (l)). By further increasing the dilution, the system show a clear chimera PS1-PS2 state over a range $0.3 \le d \le 0.5$. For $d > 0.5$ the two attractors merge in a commons PS state, analogously to the previously considered set of parameters (as shown in Fig. 1.4 (d)(h)(p) and (r) for $d = 0.8$).

In this latter case we also measured the maximal Lyapunov exponent λ^M and we observed that it stays positive for all the considered dilution values (see inset Fig. 1.4(b)). However, while for vanishing dilutions the origin of the chaotic dynamics can be considered as a collective effect induced by the chaotic motion of the coupled macroscopic fields, analogous to the chaotic state observed for two fully coupled populations [12], for larger dilution we expect chaotic effects to be present at the level of the single populations, in the form of (microscopic) *weak chaos*. This form of chaos disappears in the thermodynamic limit, and it is due to stochastic fluctuations of the single macroscopic fields induced by finite in-degree effects [11, 2]. At intermediate dilution both effects are present and the level of chaoticity is bigger with respect to the fully coupled case (where, $\lambda_M \simeq 0.02$); this is also evident from Fig. 1.4 (b) where one attractor appears as being chaotic, while the other is in a PS state plus finite size fluctuations. To summarize, the system in absence of dilution, thanks to the interaction of the two populations, exhibits *collective chaos*, the dilution induces another form of chaos termed *weak chaos*, because it present only in systems of finite size. However, for the chosen system size and parameters the level of chaoticity due to finite size fluctuations is definitely higher than that due to collective chaos.
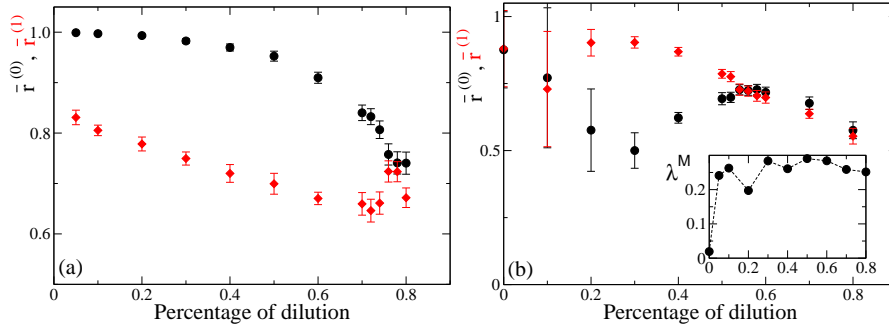
Fig. 1.5 (Color Online) In panels (a), (b) are reported the average values of the order parameters $\bar{r}^{(0)}$ and $\bar{r}^{(1)}$ as a function of the percentage of dilution. In the inset is reported the maximum Lyapunov exponent as a function of the percentage of dilution. As regards the parameter values, $(g_c = 0.04, g_s = 0.1)$ in (a) and $(g_c = 0.08, g_s = 0.16)$ in (b).

1.5 Noisy Dynamics

In this case, we consider as unperturbed state a network with a small level of dilution $d = 0.2$ and we study how the noise modify the original dynamics. In absence of noise we consider once more a chimera PS-FS state and a chaotic state. Please, notice that the small dilution modifies the phase diagram shown in Fig.1.1 for the globally coupled case. In particular in order to observe a chaotic symmetric state, we have been forced to employ parameter values slightly different from those considered in the previous Section for the same state, namely we used $(g_c = 0.08, g_s = 0.2)$.

For the chimera FS-PS, it is evident from Fig. 1.7 (a) that the complete synchronization in one population persist only up to noise of amplitudes $\Delta \simeq 0.02$, however the two populations behave differently over a quite wide range of noise amplitudes (namely, $0 \leq \Delta \leq 0.07$). In all this range we observe chimera states of the type PS1-PS2, obviously with fluctuations in the macroscopic variables induced by noise, as it is evident from Fig. 1.6 (a), (e), (i), and (o). By further increasing the noise amplitude a complete symmetry is recovered but the fields still exhibit periodic collective oscillations as shown in Fig. 1.6 (q). Also all the other indicators suggest that each population is still PS, in particular the synchronization degree remains quite high $\bar{r}^{(0)}, \bar{r}^{(1)} \simeq 0.8$ (see also Figs 1.6 (c),(g), (m) and (q)).

For what concerns the chaotic state, this remains symmetric and characterized by an unique chaotic attractor up to noises of quite large amplitude, namely $\Delta = 0.05$. As evident, from Figs. 1.6 (b),(f),(l) and (p), all the characteristics of a collectively chaotic state seems present: overlapping chaotic attractors filling a closed portion of the phase space, anti-phase irregular oscillations in the order parameters over long time scales etc. The quite unexpected result is that by further increasing noise the symmetry of the attractors is broken and the system evolves towards a chimera PS1-PS2 state, which is observable in the range $0.06 \leq \Delta \leq 0.08$ (as shown in Fig. 1.7 (b)). A specific example of this broken symmetry state is reported in Figs. 1.6 (d),(h),(n) and (r) for $\Delta = 0.08$. For even larger noise amplitudes the two attractors converge towards a common PS state with level of average synchronization $\bar{r} \simeq 0.6$.

1.6 Discussion

A first important aspect to notice, is that in the present model the Chimera states FS-PS and PS1-PS2 do not coexist with a stable regime where both populations are FS, as usual for Chimera states emerging in phase oscillator populations. This implies that in the present case the initial conditions should not be prepared in some peculiar way to observe the emergence of broken symmetry states, therefore they are not induced by the choice of the initial conditions as in most of the examined models. Spontaneously emerging Chimera, in system where the FS was unstable, have been reported also for chains of Hodgkin-Huxley neurons [18] and of Stuart-Landau oscillators [5].
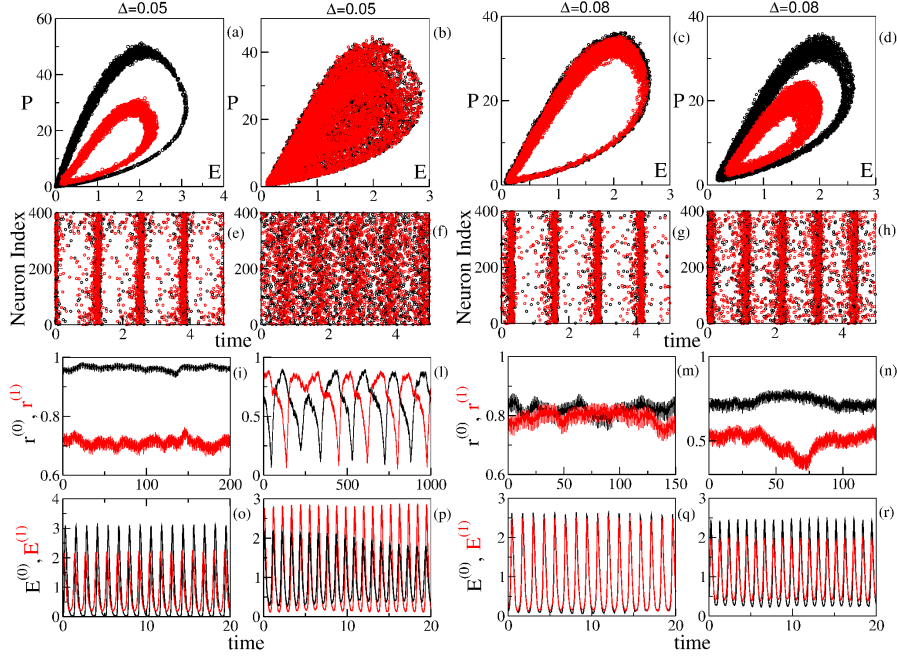
Fig. 1.6 (Color Online) **Noise Influence.** Macroscopic and microscopic characterization for two different noise amplitudes, (namely, $\Delta = 0.05$ and 0.08) of two states that for $\Delta \to 0$ and $d = 0.2$ were FS-PS (first and third columns) and chaotic (second and fourth columns). In the rows the same variables as in Fig. 1.4 are displayed. Macroscopic attractors displayed by reporting The variables corresponding to population 0 (resp. 1) are shown in black (resp. red). As regards the parameter values, $(g_c = 0.04, g_s = 0.1)$ for first and third columns, and $(g_c = 0.08, g_s = 0.2)$ for second and fourth columns. The employed noise amplitude are reported above the corresponding columns. In all cases the dilution was fixed to $d = 0.2$ and $N = 400$.
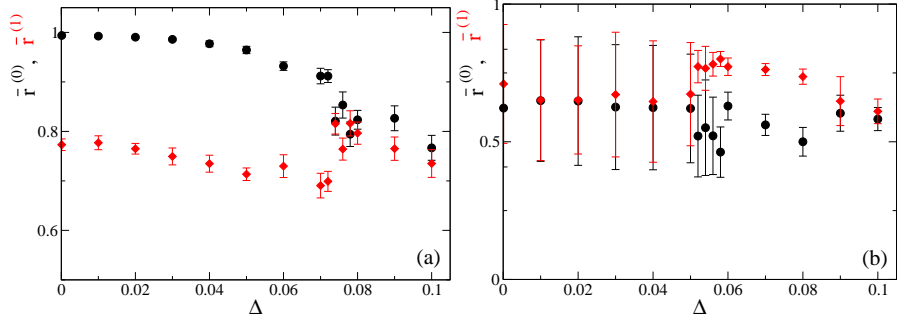
Fig. 1.7 (Color Online) In panels (a), (b) are reported the average values of the order parameters $\bar{r}^{(0)}$ and $\bar{r}^{(1)}$ as a function of the noise Δ. As regards the parameter values, $(g_c = 0.04, g_s = 0.1)$ in (a) and $(g_c = 0.08, g_s = 0.2)$ in (b). In both cases the dilution is $d = 0.2$.

As general results, we observe that dilution or noise have a similar influence on the studied macroscopic dynamics, despite random dilution represents a quenched form of disorder, while dynamical noise an annealed one. In particular, starting from a broken symmetry state dilution or noise reduce the level of synchronization in the two population, leading the dynamics of the two networks to be more and more similar for increasing dilution/noise. On the other hand, starting from a symmetric state, namely a chaotic one, the role of disorder is to break (at some intermediate dilution or noise amplitude) the symmetry among the dynamics of the two populations. Thus in this case, the disorder can promote the emergence of a chimera-like state (a PS1-PS2) in a range of parameters where the dynamics was fully symmetric in the globally coupled deterministic set-up. For large dilution/noise the system always ends up in a partially synchronized regime. This can be explained by the fact that the stable state, for the chosen parameter and for identical coupling among neurons of both populations (namely, $g_s = g_c$), is the regime PS. Indeed, for large dilution or noise the heterogeneity in the synaptic coupling among neurons lying in one population or in another become less pronounced and the PS emerge. Thefer-ore, disorder has at some intermediate level a constructive effect inducing the birth of a more complex (broken symmetry) state from a fully symmetric one, similarly to what reported in [19], where *coherence-resonance chimeras* have been observed.

Another interesting aspect, is that the chimera-like states PS1-PS2 are quite robust to dilution, they can be observed up to 80% of randomly broken links within each population, while previous results on phase oscillators pointed out that chimeras are observable up to 8% of dilution [6]. The origin of this noticeably difference is probably due to the fact that in this model PS states can be observed even in sparse networks with an extremely small in-degree ($K \simeq 10$) as shown in [9]. Furthermore, another stabilizing factor is the choice of the cross synaptic current, in our model the effect of one population on the neurons of the other population is mimicked via a macroscopic mean field, representing the average synaptic current.

The reported results represent only a first step in the study of the emergence of chimera states in neural systems characterized by a sparse topology and by the presence of noise. Further analysis will be required to investigate more realistic models and to understand if chimera states can have a role in the encoding of information at a population level in brain circuits.

Appendix: Accurate event driven map for the two fully coupled populations

In the two symmetrically fully coupled populations setup here discussed we find various kind of symmetric and symmetry broken states; in particular we find synchronized states. The integration of such states can be become a difficult issue, due to numerical round-off it can become extremely difficult to determine the next firing neuron, thus to increase the numerical accuracy and to avoid spurious clustering due to numerical round-off, we implemented the following integration scheme.

In particular, instead of integrating the membrane potentials, we performed the integration of the logarithm of the difference of two successive neurons. This transformation is uniquely defined in globally coupled systems, since the order of the neurons passing threshold is preserved in time. Therefore, it is possible to define an ordered list of the potentials and, on this basis, to define uniquely the "neighbours" of a neuron. Given a set of N membrane potentials $\left\{ x_j^{(k)} \right\}_{j=1,\ldots,N}$, with $k = 0, 1$ depending on the considered family, we introduce at a generic time t the following $N + 1$ auxiliary variables:

$$
\begin{aligned}
\omega_1^{(k)}(t) &= \ln\left[1 - x_1^{(k)}(t) \right] \\
\omega_j^{(k)}(t) &= \ln\left[x_{j-1}^{(k)}(t) - x_j^{(k)}(t) \right] \qquad j = 2, \ldots, N \\
\omega_{N+1}^{(k)}(t) &= \ln\left[x_N^{(k)}(t) \right]
\end{aligned}
$$

where the threshold (resp. reset) value is $x_{th} = 1$ (resp. $x_R = 0$) and $x_1^{(k)}$ is the next to threshold neuron.

Since we would like to define an event driven map for the two coupled families, it is necessary to find which neuron is going to fire next and then evolve the membrane potentials of the two populations untile the successive spike emission. The evolution of the two populations is different and it depends on the fact that the firing neuron belongs to the considered family or not. Let us schematize the algorithm in three steps:

1. As a first step we compare $x_1^{(0)}$ with $x_1^{(1)}$ to identify to which family the firing neuron belongs.
2. As a second step we check if the firing neuron belongs to a family which has already fired at the previous event or not. Depending on this, we have two possible alternatives: if the next and previous firing neurons belong to the same family we iterate the network as in point (a) below, otherwise as in point (b).

   a. Let us suppose that the firing population is the family (0). We evolve all the $N + 1$ variables $\left\{ \omega_j^{(0)} \right\}_{j=1,\ldots,N+1}$ for the firing family, while, for the other family, it is sufficient to evolve just the variables $\omega_1^{(1)}$ and $\omega_{N+1}^{(1)}$. All the above

mentioned variables are evolved for a lapse of time corresponding to the interval elapsed from the last firing event of the family (0).

b. If the firing family is (1) and previously fired a neuron of family (0), the evolution is more complicated. The variables $\omega_1^{(k)}$ and $\omega_{N+1}^{(k)}$ of both families are integrated for the time interval elapsed from the last firing time of family (0). The $N-1$ variables $\left\{\omega_j^{(1)}\right\}_{j=2,\dots,N}$ should be instead evolved for a longer time corresponding to the last interspike interval associated to family (1), because these variables have not been updated since the last firing of family (1).

3. The firing family is iterated in the comoving frame: this amounts to update the membrane potentials and to shift the index of all neurons by one unit. The membrane potentials of the other family are updated in the fixed reference frame.
4. The simulation is iterated by repeating the above three steps.

In order to evolve the a linearized system the previous algorithm is no more effective since now it is necessary to evolve all the variables at each time step in order to calculate the linearized equations in the tangent space. In this case we use directly the difference of the membrane potentials of two successive neurons instead of the logarithm. We still search for the first to fire neuron between the two populations and we treat differently the variables of the two populations at each time step depending on which neuron has emitted a spike previously. As in the previous case we employ different reference frames for the firing or not firing family (see point 3 above).

References

1. Abrams D.M., Mirollo R.E., Strogatz S.H., Wiley D.A., Phys. Rev. Lett. **101**, 084103 (2008).
2. Angulo-Garcia D. and Torcini A., Phys. Rev. E **91**, 022928 (2015).
3. Aurell E., Boffetta G., Crisanti A., Paladin G., Vulpiani A., Phys. Rev. Lett. **77**, 1262 (1996).
4. Bolotov M.I., Osipov G.V., Pikovsky A., Phys. Rev. E **93**, 032202 (2016).
5. Bordyugov G., Pikovsky A. and Rosenblum M., Phys. Rev. E **82**, 035205 (2010).
6. Laing C. R., Rajendran K. and Kevrekidis I. G., Chaos **22**, 013132 (2012).
7. Laing C. R., Chaos **22**, 043104 (2012).
8. Loos S. A., Claussen J. C., Schöll E. and Zakharova A., Phys. Rev. E **93** 012209 (2016)
9. Luccioli S., Olmi S., Politi, and Torcini A., Physical Rev. Lett. **109** 138103 (2012).
10. Nakagawa N., Kuramoto Y., Physica **80D**, 307 (1995).
11. Olmi S., Livi R., Politi A., Torcini A., Phys. Rev. E **81**, 046119 (2010).
12. Olmi S., Politi A., Torcini A., EPL (Europhysics Letters) **92** (6), 60007 (2010).
13. Olmi S., Chaos **25**, 123125 (2015).
14. Panaggio M. K. and Abrams D. M., Nonlinearity **28**, R67 (2015).
15. Pazó D., Montbrió E., Physical Review X **4**, 011009 (2014).
16. Pikovsky A., Rosenblum M., Phys. Rev. Lett. **101**, 264103 (2008).
17. Rothkegel A., Lehnertz K., New Journal of Physics **16**, 055006 (2014).
18. Sakaguchi H., Phys. Rev. E **73**, 031907 (2006).
19. Semenova N., Zakharova A., Anishchenko V., Schöll E., arXiv:1512.07036 (2015).
20. Tsigkri-DeSmedt N. D., Hizanidis J., Hövel P., Provata A, Procedia Computer Science **66**, 13-22 (2015).

21. van Vreeswijk C., Phys. Rev. E **54**, 5522 (1996).
22. Winfree A.T., *The Geometry of Biological Time*, (Springer Verlag, Berlin, 1980).
23. Zillmer R., Livi R., Politi A., Torcini A., Phys. Rev. E **76**, 046102 (2007).